Atmospheric aerosol and water vapor characteristics over north central Canada during BOREAS

B. L. Markham, J. S. Schafer,[1] and B. N. Holben

Biospheric Sciences Branch, NASA Goddard Space Flight Center, Greenbelt, Maryland

R. N. Halthore[2]

Department of Applied Sciences, Brookhaven National Laboratories, Upton, New York

Abstract. A network of five automated and two handheld solar radiometers was operated during the 1994–1996 Boreal Ecosystem-Atmosphere Study (BOREAS) in northern Saskatchewan and Manitoba, Canada, in order to characterize the atmospheric aerosol properties. Direct solar measurements were used to measure atmospheric transmission and infer aerosol optical thickness and water vapor column abundance. Near-Sun sky radiance measurements (solar aureole) were used to estimate the aerosol size distribution. Aerosol conditions were heavily influenced by the presence or absence of forest fires. In 1996, when few fires occurred, conditions were uniform across the region with median aerosol optical thickness (AOT) at 500 nm of 0.12 and 90th percentile values of 0.27 for the May–October period. During the 1994 and 1995 seasons, numerous fires occurred in the vicinity of the sites. The median AOT values were comparable with the 1996 values, though the 90th percentile values were larger, in general measuring 0.85 (southern 1994 season was 0.43). Median column water vapor measurements for the same 7 month period were in the range from 1.32 to 1.58 cm at both sites, with 1995 being the driest year of observation. Winter median values of AOT and water vapor were typically 0.09 and 0.34 cm, respectively. Size distributions derived from solar almucantar measurements show the predominance of small particles during smoke episodes when compared to that for background conditions. Spectral dependence of the AOT as characterized by the wavelength exponent, α, asymptotes at 1.8 for high optical depths for a 7 month season of cloud-screened data at the northern young jack pine site. This observed wavelength exponent for boreal biomass burning conditions is within the range of values found during the burning season in a study in Brazil.

Introduction

Aerosol optical properties and atmospheric water vapor transmission constitute major uncertainties in remote estimations of the ground properties such as reflectance and temperature due to the variable nature of the aerosol and water vapor sources and associated dispersive mechanisms [Lenoble, 1993]. Variation in atmospheric aerosols is second only to greenhouse gases as a known mechanism for global climate forcing [Hansen and Lacis, 1990]. Even so, the net radiative effect of atmospheric aerosols on global climate via backscatter to space of solar radiation to space or changes in cloud albedo by microphysical processes [Twomey, 1991] is still not fully understood [Hegg et al., 1995; Schwartz, 1996]. This is due in part to poor spatial continuity of tropospheric aerosol data used to parameterize global radiative forcing models [d'Almeida and Koepke, 1988]. Records of aerosol characteristics for many regions of the world are determined from short-term localized studies or frequently are absent altogether. Some extensive aerosol stud-

ies have been conducted in the central U.S. plains [Bruegge et al., 1992b; Halthore et al., 1992a] and in the province of Ontario, Canada [Ahern et al., 1991]. However, previous studies of this nature have not provided an opportunity for characterizing aerosols in the boreal forest region with its typical seasonal forest fire activity.

The objective of this study was to characterize the aerosol and water vapor content of the atmosphere over the region where the BOREAS studies were being conducted. Specifically, aerosol spectral optical thickness, size distribution, and scattering phase function, as well as column water vapor amount, were to be determined. No attempt was made to measure the albedo of single scatter of the aerosol particles as a part of this study. This remains a significant unknown as the absorption properties of smoke particles vary with the combustion efficiency of the biomass burning [Kaufman et al., 1994; Ward et al., 1992]. To date, this study has spanned 1994–1996, the period when the bulk of the BOREAS studies have been conducted but may be extended. Such a multiyear record of high-frequency aerosol measurements taken during conditions ranging from very clean air to that of high smoke content should prove to be a valuable data set for broadening the base of aerosol climatology. It is believed to be the first extensive study of aerosol characteristics over the central Canadian boreal forest region.

---

[1]Now at Hughes STX Corporation, Greenbelt, Maryland.
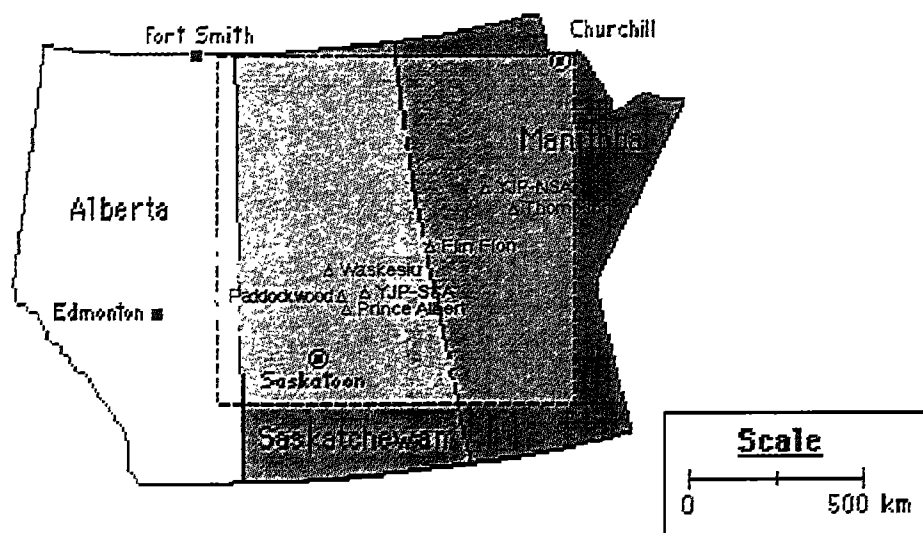[2]Formerly at HSTX/GSFC-NASA, Greenbelt, Maryland

Figure 1. Sun photometer locations in the BOREAS study area.

Method

The BOREAS region, shown in Figure 1, was divided into a northern study area (NSA) in Manitoba and a southern study area (SSA) in Saskatchewan. These areas, separated by about 600 km, are representative of the southern and the northern limits of the boreal forest. Each of the study areas contained a number of subsites in different vegetation types. These two areas are relatively free of human sources of aerosols. Logging activity can be seen throughout the SSA with a major paper mill located outside the southern edge of the SSA. To the east of the NSA is a large nickel smelting operation at Thompson, Manitoba. A similar operation exists at Flin Flon, Manitoba, which is midway between the two study areas. Forest fires are common in the region during the summer months.

To obtain aerosol properties over this large area, a complement of five automatic Sun and sky-scanning radiometers and two handheld Sun photometers were used. In 1994, four of the automatic instruments were distributed along a transect between the NSA and the SSA with one in the NSA at the young jack pine (YJP) site, one at the airport in Flin Flon (between SSA and NSA), one in the eastern portion of the SSA at the young jack pine site, and one in the western part of SSA at Waskesiu Lake in the Prince Albert National Park (PANP). A fifth one was used during the intensive field campaigns at the Prince Albert Airport slightly to the south of the SSA and at the Thompson Airport in the NSA. In 1995 the same sites were used, though the fifth instrument remained at Thompson, Manitoba, for the duration of the field season. In 1996 the Flin Flon site was replaced with a third SSA site at Paddockwood (Figure 1). For all campaigns these five radiometers were deployed from approximately May to October. The handheld Sun photometers were located at Thompson and PANP. These provided data throughout the year, including the winter months in which observations were made once daily at SPOT satellite overpass time (~1800 UT) and at SPOT, Landsat, and NOAA 9/11 overpass times during spring and fall. Tables 1 and 2 display the operational periods of the instruments in 1994, 1995, and 1996 for the automatic Sun photometers and handheld Sun photometers, respectively.

Instrument Description

The automatic Sun photometers (model CE-318A) were manufactured by CIMEL Electronique. During 1994 they were equipped with 10 nm band-pass filters in the visible and near infrared with center wavelengths at 340, 380, 440, 670, 870, 940, and 1020 and an additional 50 nm band-pass filter centered at 940 nm. The two 940 nm channels were to be used for column water abundance determination. The wider band-pass filter proved unnecessary for the determination of water vapor column abundance and was more sensitive to atmospheric conditions such as environmental lapse rate and water vapor profile [*Halthore et al.*, 1997]. Thus it was replaced with a 10 nm band-pass filter centered at 500 nm in spring 1995. In addition

Table 1. Operation Periods for Cimel Automatic Sun Photometers During 1994, 1995, and 1996 BOREAS Campaigns

	Operation Periods
1994	
Flin-Flon, MB	5/19–10/13
NSA-young jack pine	5/18–11/01
SSA-young jack pine	5/23–10/13
Waskesiu, SK	5/25–10/13
Thompson, MB	6/08–6/13, 7/27–9/10
Prince Albert, SK	5/17–6/06, 7/20–7/26, 9/12–9/18
1995	
Flin-Flon, MB	5/18–9/07
NSA-young jack pine	5/16–11/3
SSA-young jack pine	5/25–6/01, 7/01–11/21
Waskesiu, SK	5/24–8/01, 8/22–11/04
Thompson, MB	5/15–10/29
1996	
Paddockwood, SK	2/27–11/07
NSA-young jack pine	5/14–9/24, 9/30–10/09
SSA-young jack pine	5/10–5/14, 5/28–9/20, 10/01–10/23
Waskesiu, SK	5/08–5/14, 5/23–9/04, 9/29–10/27
Thompson, MB	5/14–10/09

MB, Manitoba; SK, Saskatchewan.
Read 5/19–10/13 as May 19 to October 13.

Table 2. Operation Periods for Handheld Sun Photometers During 1994, 1995, and 1996 BOREAS Campaigns

	Operation Periods
1994	
Waskesiu, SK	1/04–3/03, 3/22–9/26, 10/10–12/22
Thompson, MB	1/01–6/29, 8/01–10/21
1995	
Waskesiu, SK	1/01–4/11, 5/04–9/02, 9/21–10/08
Thompson, MB	2/04–12/20
1996	
Waskesiu, SK	1/03–present
Thompson, MB	1/03–present

Gaps may indicate extended cloudy conditions, instrument problems, or operator unavailability.

to the direct solar irradiance measurements that are made with a field of view of 1.2°, these instruments measure the sky radiance in four spectral bands (440, 670, 870, and 1020 nm) along the solar principal plane (i.e., at constant azimuth angle, with varied solar zenith angles) up to 9 times a day and along the solar almucantar (i.e., at constant solar zenith angle, with varied azimuth angles) up to 6 times a day. A preprogramed sequence of measurements is taken by these instruments starting at an air mass of 7 in the morning and ending at an air mass of 7 in the evening. Air mass is calculated according to Kasten's equation [Kasten and Young, 1989]. During the large air mass

periods, direct Sun measurements are made at 0.25 air mass intervals, while at smaller air masses, the interval between measurements is typically 15 min. The almucantar measurements are taken at 0.5° intervals near the Sun (within 6°) and increase from 2° to 10° intervals away from the solar position. The data are collected and transmitted via GOES satellite at 1 hour intervals to a computer at the Wallops Island facility [Holben et al., 1996]. The data were analyzed on a daily basis for aerosol optical thickness, water column abundance, and aerosol size distribution.

The two handheld Sun photometers have four channels (500, 670, 870, and 940 nm). They are capable of only the direct solar measurements and require manual data entry. They have a peak hold feature that allows them to record the highest voltage response when pointed in the general direction of the Sun. These instruments have been used continuously from June 1993 through the 1996 field campaign and are still in use, primarily to characterize the atmosphere during satellite overpass times.

Calibration

Automatic instruments from the Goddard Space Flight Center (GSFC) were regularly taken to the Mauna Loa Observatory in Hawaii, where the Langley method [Shaw, 1983] was used for absolute calibration of these reference Sun photometers. Instruments used for BOREAS were calibrated by intercomparison with reference instruments with measurements conducted on the top of a building at GFSC on clear days with
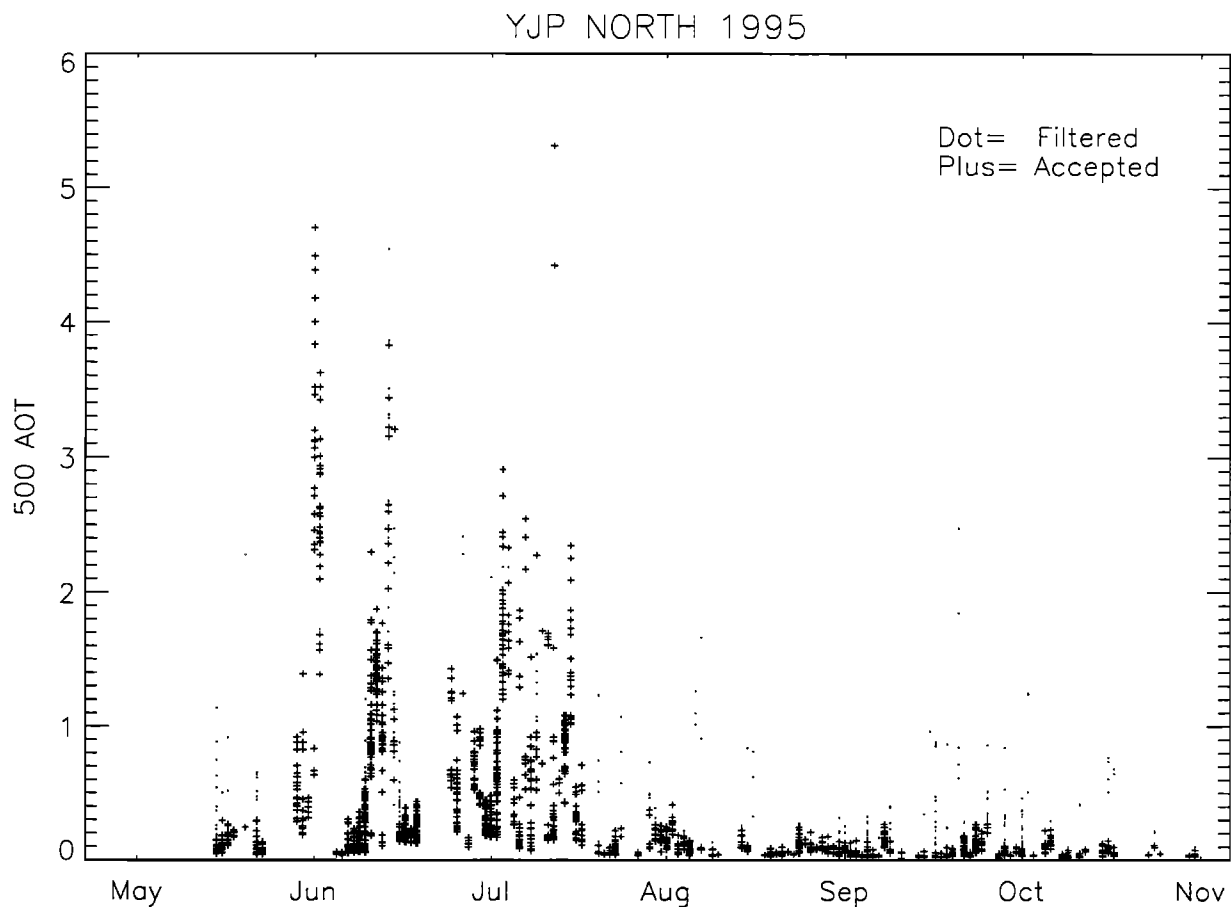

Figure 2. Aerosol optical thickness at 500 nm for the 1995 season at YJP-NSA. Observations excluded by cloud-screening procedures are designated.
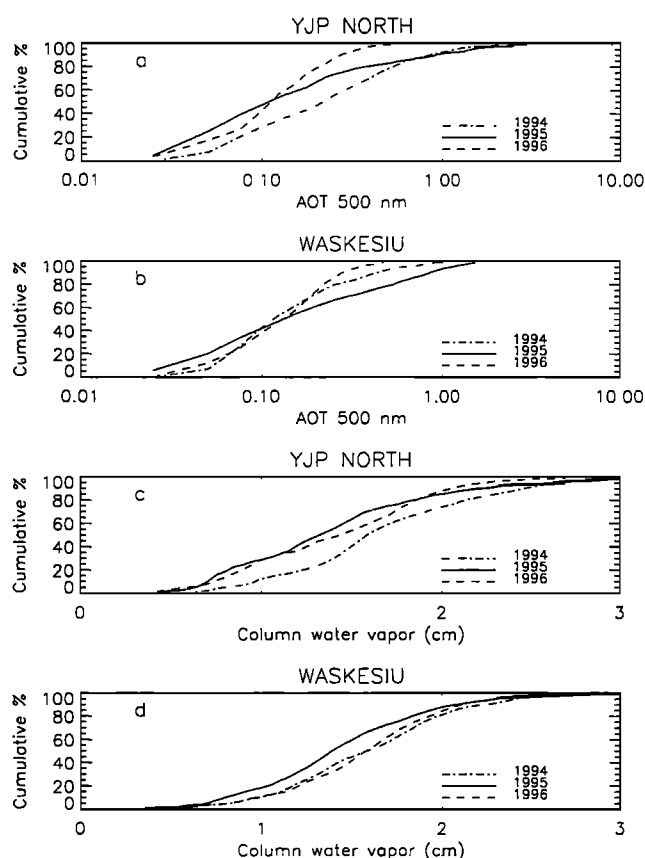
YJP NORTH

WASKESIU

YJP NORTH

WASKESIU

Figure 3. Cumulative percentage histograms for three seasons. (a) YJP-NSA AOT 500 nm, (b) Waskesiu AOT 500 nm, (c) YJP-NSA column water vapor (centimeters), and (d) Waskesiu column water vapor (centimeters).

low aerosol loading. If the aerosol conditions were considered to be constant during the Langley procedures at Mauna Loa, then deviation of measurements from the linear regression line gives an indication of the Sun photometer precision. The CI-MEL's make three direct Sun measurements at each wavelength in a 30 s scan sequence. This group of three measurements is referred to as a triplet. The coefficient of variability of the triplets for three reference instruments deployed at Mauna Loa were calculated on the basis of 168, 264, and 288 observations, respectively. For all wavelengths the variability of a triplet was always less than 1% and generally about 0.3%, giving an estimate of the instrument's reproducibility [*Holben et al.*, 1996]. The calibration coefficients, values of V_0, are usually determined by averaging the y intercepts from three to seven Langley plots at Mauna Loa Observatory. The averaged V_0 values from all calibration sessions at Mauna Loa have a coefficient of variability of ~0.25–0.5% for the visible and near-IR wavelengths, ~0.5–2% for the UV, and ~1.0–3.0% for the water vapor channel [*Holben et al.*, 1996]. The overall accuracy of aerosol optical thickness measurements is expected to be in the range of ±0.02 at an air mass of 1.0. The handheld Sun photometers were calibrated by intercomparison with co-located CIMEL's. The estimated level of uncertainty for these instruments is greater (±0.04) due to less frequent recalibration. For the sky radiance measurements, calibration was performed at the NASA Goddard Calibration Facility using a calibrated integrating sphere to an accuracy of ±5%. For the

940 nm channel, which includes water absorption, calibration was performed by using a variant of the modified Langley method as described by *Halthore et al.* [1997]. The method used is similar to that described elsewhere [*Bruegge et al.*, 1992b; *Halthore et al.*, 1992b]. Column amounts of precipitable water derived from Sun photometer measurements at BOREAS have compared favorably with radiosonde observations [*Halthore et al.*, 1997] to within ±10%, the generally accepted accuracy of radiosonde measurements.

Optical thickness is calculated from spectral extinction of direct beam radiation at each wavelength based on the Beer-Bouguer Law:

$$V_\lambda = V_{o\lambda} R^{-2} e^{-(m\tau)}$$

where

V_λ digital voltage measured at wavelength (λ);
$V_{o\lambda}$ extraterrestrial voltage;
m optical air mass;
τ total vertical optical thickness;
R relative earth-Sun distance in AU.

Attenuation due to Rayleigh scatter, and absorption by ozone (from interpolated ozone climatology atlas [*London et al.*, 1976]) and gaseous pollutants, is estimated and removed to isolate the aerosol optical thickness (τ_a). Sky radiance measurements are inverted with radiative transfer equations [*Nakajima et al.*, 1983] to provide aerosol properties of size distribution and phase function over the particle size range of 0.1–5 μm.

Data Screening and Analysis

For the manual instruments, data were collected under predominantly clear sky conditions. At times, data were collected even when some cirrus clouds were present especially in the early part of the 1994 campaign. The automatic CIMEL radiometers acquire data regardless of sky conditions, except for rain, thus requiring cloud-screening procedures. Three quality control schemes are considered to reject data obtained under marginal conditions. The CIMEL's perform three scan sequences spaced 30 s apart and thus acquire three aerosol optical thickness measurements at each wavelength. If the coefficient of variation of such a triplet exceeds 12% at any

Table 3. Values Representing 50th and 90th Percentiles of May–October Measurements of Aerosol Optical Thickness (top) and Column Water Vapor (bottom) for Three Years at Two Sites

	1994	1995	1996
Aerosol Optical Thickness			
YJP north			
50%	0.22	0.12	0.11
90%	0.84	0.92	0.28
Waskesiu			
50%	0.12	0.13	0.13
90%	0.44	0.86	0.28
Column Water Vapor			
YJP north			
50%	1.58	1.32	1.44
90%	2.46	2.22	2.05
Waskesiu			
50%	1.58	1.39	1.57
90%	2.24	2.08	2.11

wavelength, the data derived from all channels are rejected. Second, data exhibiting an increasing or nearly flat aerosol optical thickness with wavelength between 440 nm and 870 nm are considered cloud contaminated. Therefore data with a wavelength exponent α less than or equal to zero are removed. For this procedure the wavelength exponent is calculated by the following:

$$\alpha = -\frac{\Delta \ln \tau_a}{\Delta \ln \lambda} \quad \text{for } \tau_a \text{ at 440 nm and 870 nm.}$$

Finally, the remaining data are plotted along with the direct Sun observations acquired during almucantar measurements that exhibited high azimuthal symmetry about the solar plane, which are expected to represent cloudless conditions. A regression line through these almucantar observations is plotted as well. The abscissa is that of aerosol optical thickness at 440 nm, while the ordinate depicts the ratio of this aerosol optical thickness to the wavelength exponent described above. The core of the remaining data set is found to follow the trend of the almucantar regression and outliers are deselected by subjectively drawn polygons.

Results and Discussion

Figure 2 displays a full season of cloud-screened aerosol optical thickness data for one wavelength at one automatic instrument site (YJP-NSA). The measurements marked with a plus have been determined to be free of cloud contamination
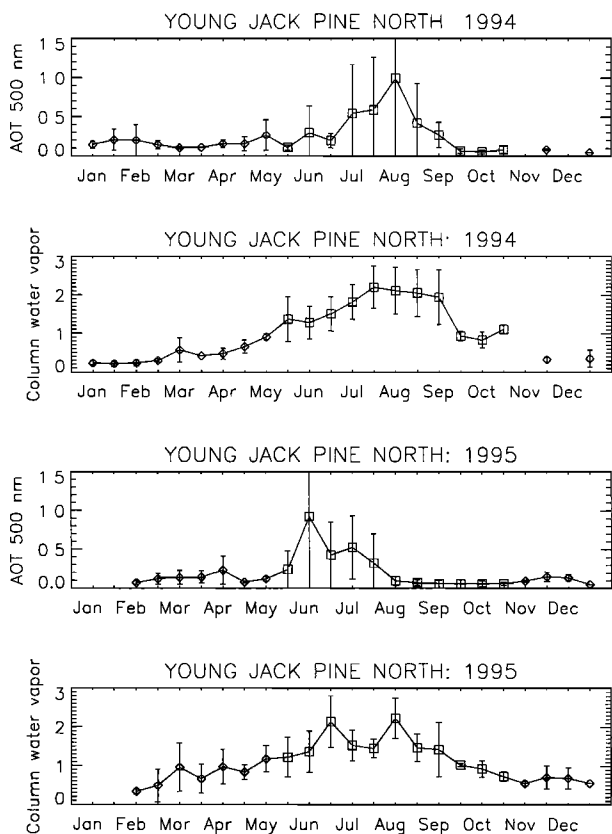

Figure 4. Midday bimonthly average of AOT (500 nm) and precipitable water for the YJP-NSA site in 1994 and 1995. Data are from Cimel Sun photometers (square) and handheld (diamond).
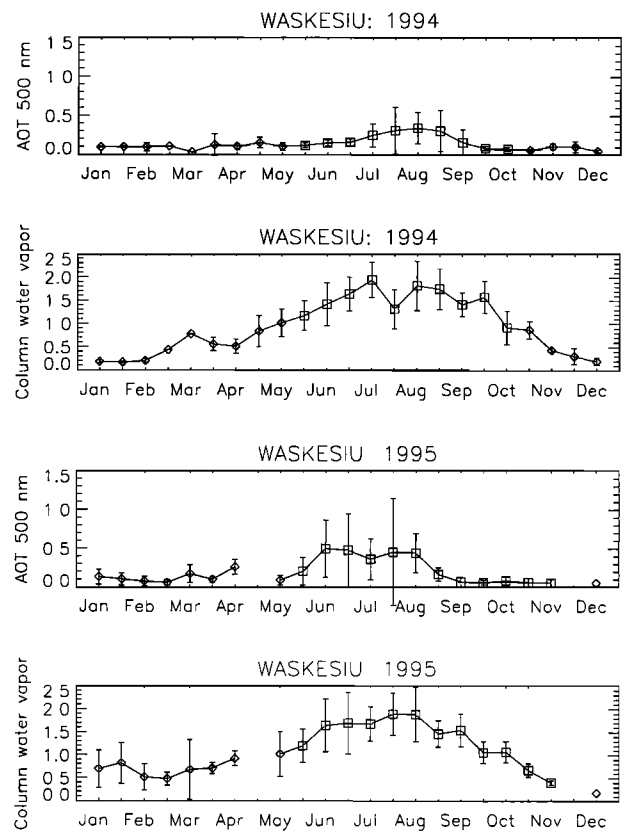

Figure 5. Midday bimonthly average of AOT (500 nm) and precipitable water for the Waskesiu site in 1994 and 1995. Data are from Cimel Sun photometers (square) and handheld (diamond).

by the cloud-screening procedure described above. Approximately 15% of the data set was excluded in this manner, with 2686 measurements retained. Figure 3 depicts the cumulative histograms of AOT at 500 nm and column water vapor for the three seasons from automatic instruments located in the northern and southern study areas. The lack of high AOT measurements during the relatively smoke-free 1996 seasons is evident. Clearly, the majority of the measurements fall below a value of 0.2 at 500 nm, with high values contributed by the forest fire episodes. Typical values in the absence of forest fires are around 0.1, whereas with fires present, values reach as high as 4.5.

The 50th and 90th percentiles of Figure 3 are given in Table 3. Except for the YJP-NSA 1994 season, the 50th percentile aerosol optical thicknesses are comparable and in the range of 0.11–0.13, implying that the median AOTs are, on the average, similar in magnitude from season to season and occur under nonsmoky conditions. For the 90th percentile the high AOTs of the burning seasons led to a disparity between 1994/1995 and the 1996 seasons. Three of the four burning seasons have 90th percentile AOTs greater than 0.8, while the 1996 seasons had values of ~0.28 at both YJP-NSA and Waskesiu sites. In fact, the AOT cumulative percentage profiles at the two sites were very similar for 1996, suggesting that the aerosols encountered across the region are, on the average, quite comparable under nonsmoky conditions.

The water vapor measurements were more consistent than AOT from year to year at both sites with low values in winter
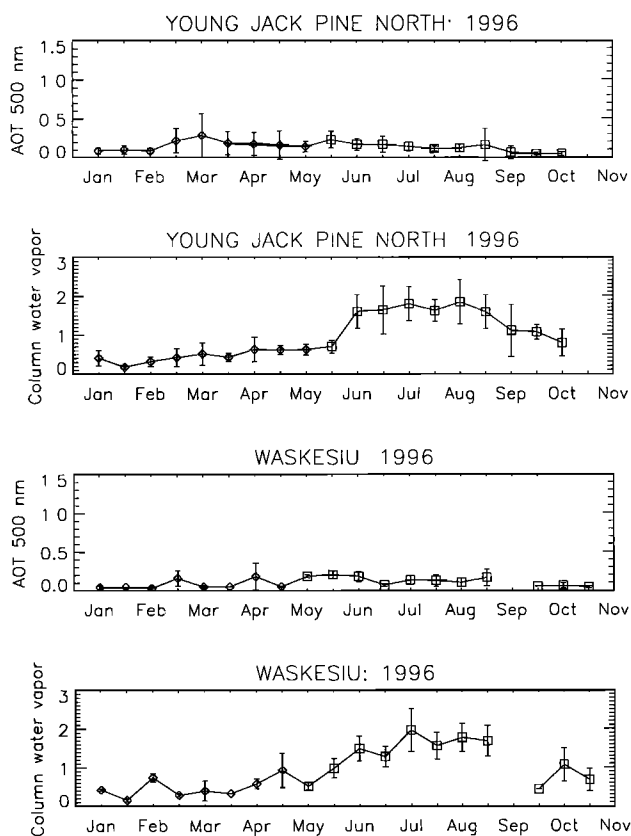
YOUNG JACK PINE NORTH· 1996

YOUNG JACK PINE NORTH 1996

WASKESIU 1996

WASKESIU: 1996

Figure 6. Midday bimonthly average of AOT (500 nm) and precipitable water for the YJP-NSA site (top) and Waskesiu site (bottom) in 1996. Data are from Cimel Sun photometers (square) and handheld (diamond).

of ~0.5 cm and larger summer values as high as 3.0 cm. Median values are given for the period of automatic instrument measurement (Table 3) and were typically ~1.5, while the 90th percentile values ranged from 2.05 to 2.46 cm.

Figures 4–6 represent semimonthly averages of aerosol optical thickness (AOT) and water vapor column abundance in the NSA and SSA for 1994, 1995, and 1996. Each figure represents the cloud-screened aerosol optical thickness data taken near midday on clear days averaged for each half of the month. Automatic instrument data are used for the period from approximately May to October (square), and handheld Sun photometer data taken at a nearby location are used for the rest of the observations (diamond). When limited data are available due to extended periods of cloudiness, or for other reasons, these averages do not represent many data points. The basic seasonal pattern for 1994 was similar for the two areas: very clear (AOT ~0.1 at 500 nm) and dry (~0.5 cm precipitable water) conditions during the winter and early spring, with hazier and higher moisture conditions during the late spring to early fall. The 1995 season displayed a similar increase in precipitable water in the summer and early fall. The forest fire activity began sooner in 1995, and this is evident in the figures as the aerosol optical thickness peaks occur from May to July, rather than July to August. The absence of a burning season in 1996 led to bimonthly averages that were less than those of the previous seasons in both the north and the south. The summer months are not distinct from the winter in Figure 6, maintaining the very low values characteristic of the nonburning season.

For the two smoky years the NSA exhibited greater magnitude and variability of aerosol optical thickness, due to a larger number of local fires. All of the plots show column water vapor profiles with roughly equivalent trends.

The size distributions of Figure 7 are a sample from successfully inverted almucantar measurements for a number of days throughout the 1994 and 1995 seasons at Waskesiu Lake, Saskatchewan (SSA). The ordinate axis represents the total volume of aerosol in a square centimeter vertical column above the instrument per unit radius interval in micrometers. Large aerosol optical thickness during smoke events is associated with a dramatic increase in the concentration of small (submicron) particles. Spatial inhomogeneity in the smoke often produced large assymetries in the almucantar aureole measurements. Such conditions made inversion during the highest smoke conditions impossible due to limitations of the radiative code. The greatest concentration of small particles in the displayed 1994 plots is seen in the size distributions of July 27 and August 2, while the maximum in the 1995 plots is that of July 3, demonstrating the earlier burning season in 1995. The predominance of small particles by more than an order of magnitude during the smoke events is apparent. The size distribu-
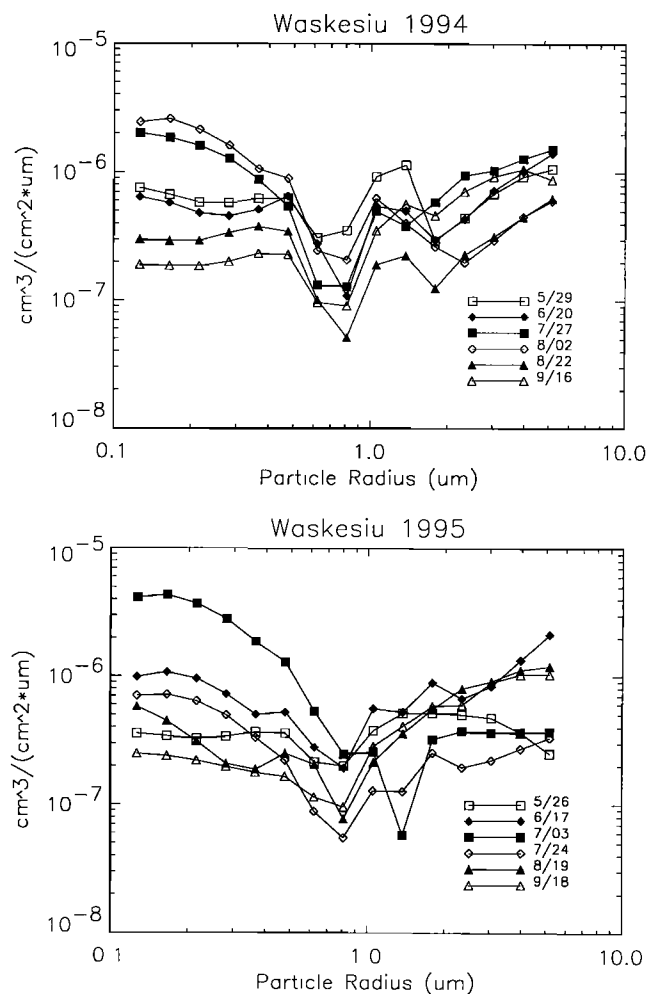
Waskesiu 1994

Waskesiu 1995

Figure 7. Size distributions at Waskesiu site obtained by inverting measured sky radiance from Cimel almucantar sequences. Ordinate value represents total aerosol volume for a square centimeter vertical column above the instrument for a unit radius interval.

tions from before and after the periods of forest fire activity exhibit much smaller particle concentrations in the submicron range. The displayed distributions taken from mid-September of each year are typical of those from the low aerosol non-burning season.

The wide range of aerosol conditions typically experienced over the season is depicted in Figure 8. The plot from September 22, 1995, at Waskesiu, Saskatchewan, shows the highly consistent, clean air conditions associated with the background aerosol, while on June 24, 1995, during heavy forest fire activity, the large aerosol optical thickness and rapid temporal variability of the atmospheric aerosol loading are evident. Changes in aerosol optical thickness at 500 nm on September 22 were often as large as 0.5 within a 30 min interval, and values were frequently more than 30 times larger than those measured on June 24.

Spatial variability is also in evidence when the burning season is under way. The diurnal trend in aerosol optical thickness at three SSA sites is plotted in Figure 9 for two days, one with a clean atmosphere (September 16, 1994) and one with localized fires (July 25, 1994). Aerosol optical thickness is generally comparable over the region (usually less than ~0.01 variation) when no burning is occurring, and the bottom plot reflects this fact. This agrees with the small spatial variation in aerosol
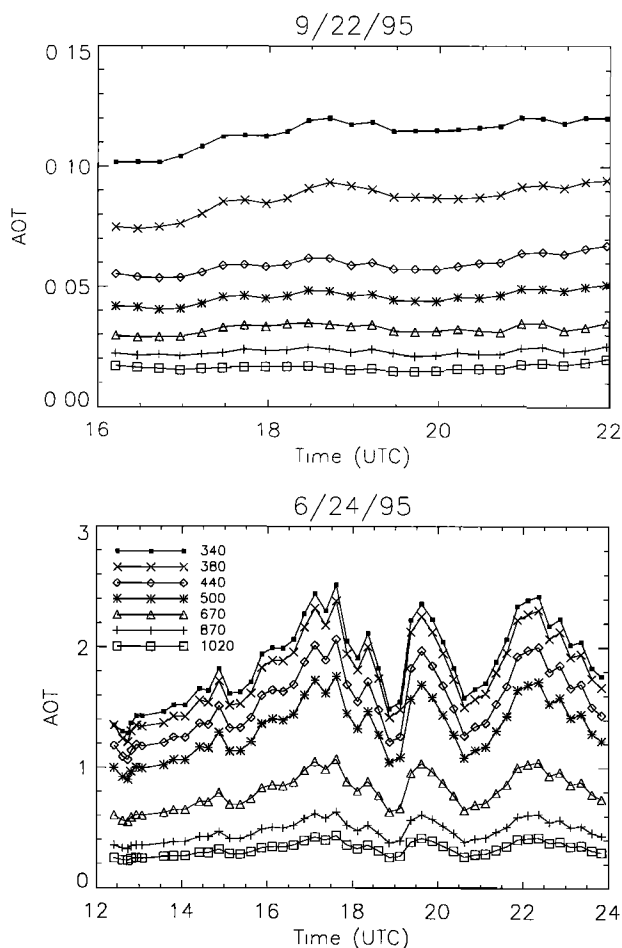

Figure 9. Observed diurnal pattern of aerosol optical thickness at 440 nm for three southern study area (SSA) sites on two days in 1994.

Figure 8. Time series of observed aerosol optical thickness at seven wavelengths at Waskesiu for a day with very clean air (September 22, 1995) and a smoke-dominated day (June 24, 1995).
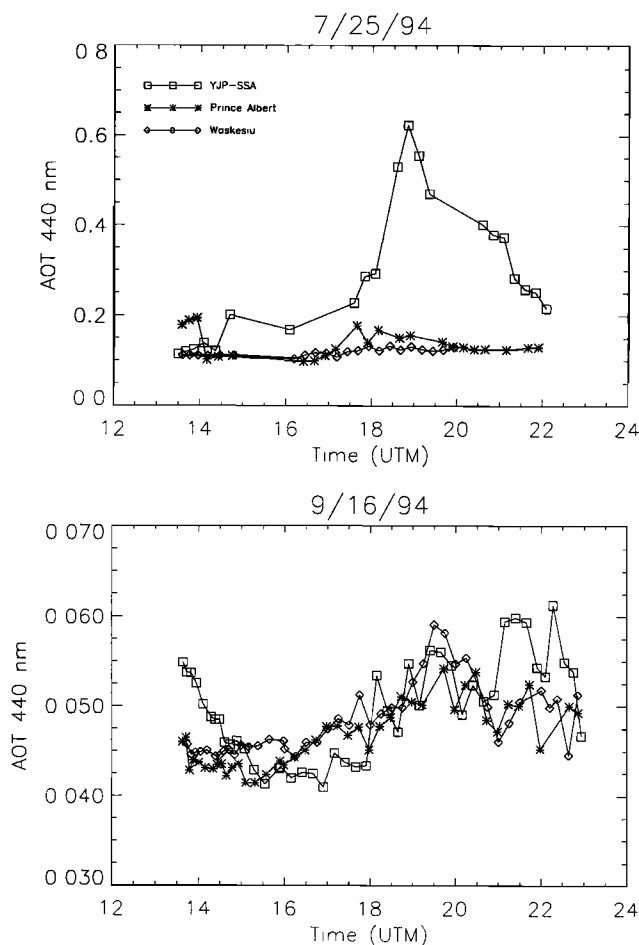
optical thickness measured on a 21 km transect over the Konza Prairie, Kansas, during the First International Satellite Land Surface Climatology Project Field Experiment (FIFE) [*Bruegge et al.*, 1992b]. A study in the Sahel region of Senegal, Mali, and Niger examined simultaneous aerosol optical thickness measurements at pairs of observation sites separated by various distances [*Holben et al.*, 1991]. Not surprisingly, the highest correlation of measurements ($r = 0.66$) was found for the two sites closest to each other (distance is 75 km). The correlation increased markedly to a value of 0.89 when the highest optical thickness cases ($\tau_a < 1.5$) were eliminated. In the Sahel region, high-aerosol optical thickness data resulted from the transport of mechanically generated dust particles into the study area, rather than smoke particles from biomass burning. When localized fires develop in the boreal forest, in this case near the YJP-SSA site, the aerosol optical thickness can differ greatly between nearby sites. The peak in the YJP-SSA time series is presumably due to the influence of a variable smoke plume from a proximal fire. Such regional variability is common throughout the periods of forest fire activity.

For each cloud-screened scan of Figure 2 the wavelength exponent α was calculated from four wavelengths, 440, 500, 670, and 870 nm, from the least squares fit slope of the natural logarithm of optical thickness as a function of the natural logarithm of the wavelength. Figure 10 is a plot of α versus
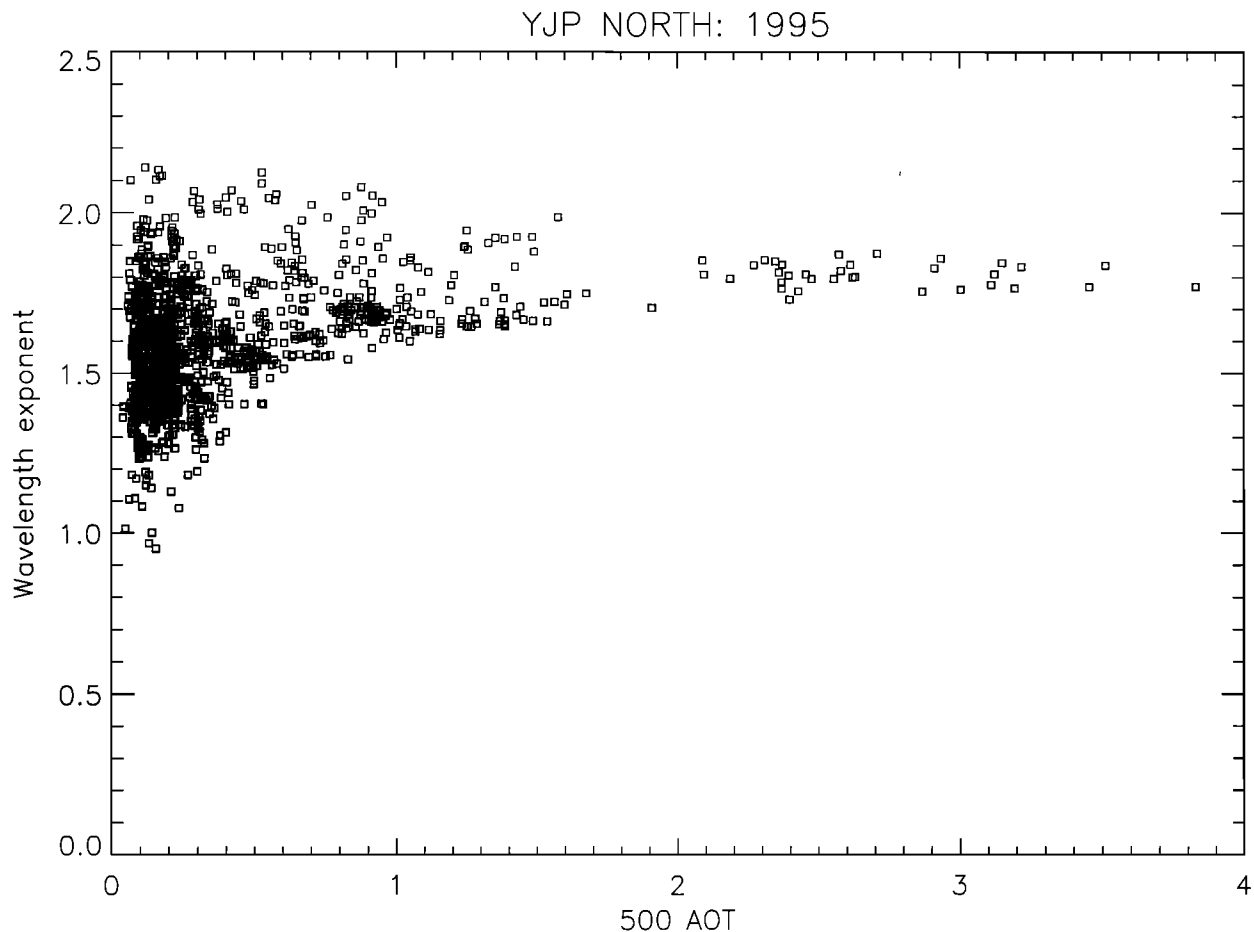
Figure 10. Wavelength exponent versus AOT at 500 nm for cloud-screened observations in 1995 at YJP-NSA site.

AOT at 500 nm at the YJP-NSA site for all cases where the least squares fit had a coefficient of correlation that was 0.99 or better. No significant correlation between α and AOT is apparent in these data. Other field experiments have shown moderate correlation between α and AOT, such as *Kaufman* [1993], with an $r^2 = 0.66$, and *Holben et al.* [1996], though little agreement between relationships for different data sets has been found. These data are more extensive, with 1094 observations, and span the 7 month CIMEL observation period of 1995 at YJP-NSA. For small to moderate AOTs (<1.0) the range of wavelength exponent is rather large. Near AOT = 1.0, the range is from 1.6 to 1.9, and for the lowest AOTs (~0.1), it varies from 1.0 to 2.1. The span of α values might reflect the variety of aerosol types and thus size distributions, which dominated the site over the course of a year. The proximity of a local nickel smelting operation (~30 km) added a possible anthropogenic source that could have resulted in low AOT measurements with high α values under certain synoptic conditions. Also, some of the variation in wavelength exponent may reflect the greater relative uncertainty of very low AOT measurements.

The higher AOTs exhibit a much smaller range of wavelength exponent centered at $\alpha = 1.8$ and are exclusively associated with biomass burning. Dominance by one primary aerosol type probably accounts for the diminished variability of this parameter. The mean value of 1.8 from the high AOT mea-

surements is comparable to the typical α values found by *Holben et al.* [1996] at their Brazilian sites during the burning season ($\alpha = 1.6$–1.9) and provides evidence that the size distributions of boreal biomass combustion products are similar to those found in the fires of tropical regions.

Using the radiative code 6S [*Vermote et al.*, 1996], a simulation study was conducted to evaluate the effect of smoke aerosols on vegetation status parameters derived from remotely sensed data. For a solar zenith angle of 37° on June 13 at 1700 UT, the apparent reflectance (ρ), in the Landsat Thematic Mapper (TM) red and infrared channels, was modeled for two greatly different aerosol size distributions. The size distributions were taken from successfully inverted almucantar measurements exhibiting good symmetry. The distribution representing clean air conditions (τ_a at 500 nm = 0.103) typical of

Table 4. Apparent Reflectance and NDVI From Radiative Code 6S as Modeled for Clear and Smoke-Dominated Aerosol Size Distributions

	ρ Smoke	ρ Clear
Landsat		
CH3	0.1601	0.1246
CH4	0.4487	0.4904
NDVI	0.474	0.595

the nonburning season was an inversion from late August of the 1995 season, while that representing smoky conditions (τ_a at 500 nm = 1.12) was acquired during mid-June of the same season.

From the calculated radiances the normalized difference vegetation index (NDVI) was determined. Table 4 contains the model output. As would be expected, the effect of smoke on calculated NDVI is significant. The presence of smoke increases the apparent reflectance at the sensor in the red channel and results in a reduction of 0.12 NDVI units (20% reduction from the clear case) for the assumed conditions. The AOT of 1.12 at 500 nm on the representative smoky day used for these calculations was the highest value recorded, with almucantar data that met the criterion of good symmetry for size distribution inversion.

Conclusions

The preceding results reflect a valuable and unique multi-year data set of aerosol optical properties and precipitable water content in north central Canada. Seasonal trends in precipitable water were, in general, similar in both study areas and for both campaign years. During smoke-free conditions the typical aerosol optical thickness is observed to be extremely small for a continental site, being occasionally as low as 0.02 at 500 nm, while values during forest fire activity can become as large as 4.5. Significant increases in small (submicron) particles produce order of magnitude changes in derived size distributions when aerosol combustion products are released by burning biomass. Wavelength exponents typically observed during boreal forest fires were quite similar to those measured during biomass burning in a Brazilian study. No significant correlation was observed between wavelength exponent and aerosol optical thickness, though smoke-dominated conditions yielded a much smaller range of α. NDVI values modeled by using actual inverted aerosol size distributions indicated a marked decrease of 0.12 NDVI units for the smoky conditions.

References

Ahern, F. J., R. P. Gauthier, P. M. Teillet, J. Sirois, G. Fedosejevs, and D. Lorente, Investigation of continental aerosols with high-spectral-resolution solar-extinction measurements, *Appl. Opt.*, *30*, 5276–5287, 1991.

Bruegge, C. T., J. E. Conel, R. O. Green, J. S. Margolis, R. G. Holm, and G. Toon, Water vapor column abundance retrievals during FIFE, *J. Geophys. Res.*, *97*, 18,759–18,768, 1992a.

Bruegge, C. T., R. N. Halthore, B. L. Markham, M. Spanner, and R. Wrigley, Aerosol optical depth retrievals over the Konza Prairie, *J. Geophys. Res.*, *97*, 18,743–18,758, 1992b.

d'Almeida, G. A., and P. Koepke, An approach to a global optical aerosol climatology, in *Aerosols and Climate*, edited by P. V. Hobbs and M. P. McCormick, A. Deepak, Hampton, Va., 1988.

Halthore, R. N., B. L. Markham, R. A. Ferrare, and T. O. Aro, Aerosol optical properties over the midcontinental United States, *J. Geophys. Res.*, *97*, 18,769–18,778, 1992a.

Halthore, R. N., B. L. Markham, and D. W. Deering, Atmospheric correction and calibration during KUREX-91, IGARSS '92, *Int. Geosci. Remote Sens. Symp.*, *2*, 1278–1280, 1992b.

Halthore, R. N., T. F. Eck, B. N. Holben, and Brian Markham, Sun photometric measurements of atmospheric water vapor column abundance in the 940-nm band, *J. Geophys. Res.*, *102*, 4343–4352, 1997.

Hansen, J. E., and A. A. Lacis, Sun and dust versus greenhouse gases: An assessment of their relative roles in global climate change, *Nature*, *345*, 713–719, 1990.

Hegg, D. A., P. V. Hobbs, R. J Ferek, and A. P. Waggoner, Measurements of some aerosol properties relevant to radiative forcing on the east coast of the United States, *J. Appl Meteorol.*, *34*, 2306–2315, 1995.

Holben, B. N., T. F. Eck, and R. S. Fraser, Temporal and spatial variability of aerosol optical depth in the Sahel region in relation to vegetation remote sensing, *Int. J. Remote Sens.*, *12*, 1147–1163, 1991.

Holben, B. N., A. Setzer, T. F. Eck, A. Pereira, and I. Slutsker, Effect of dry-season biomass burning on Amazon Basin aerosol concentrations and optical properties, 1992–1994, *J. Geophys. Res.*, *101*, 19,465–19,481, 1996.

Holben, B. N., et al., Automatic sun and sky scanning radiometer system for network aerosol monitoring, *Remote Sens. Environ.*, in press, 1997.

Kasten, F., and A. T. Young, Revised optical air mass tables: An approximation formula, *Appl. Opt.*, *28*, 4735–4738, 1989.

Kaufman, Y. J., Aerosol optical thickness and atmospheric path radiance, *J Geophys. Res.*, *98*, 2677–2692, 1993.

Kaufman, Y. J., B. N. Holben, D. Tanré, and D. E Ward, Remote sensing of biomass burning in the Amazon, *Remote Sens. Rev.*, *10*, 51–90, 1994.

Lenoble, J., *Atmospheric Radiative Transfer*, 532 pp., A. Deepak, Hampton, Va., 1993.

London, J., R. D. Bojkov, S Oltmans, and J. I. Kelley, Atlas of the global distribution of total ozone July 1957–June 1967, *NCAR Tech Note 133+STR*, 276 pp., Natl Cent for Atmos. Res., Boulder, Colo., 1976.

Nakajima, Y., M. Tanaka, and T. Yamauchi, Retrieval of the optical properties of aerosols from aureole and extinction data, *Appl Opt*, *22*, 2951–2959, 1983.

Schwartz, S. E., The whitehouse effect—shortwave radiative forcing of climate by anthropogenic aerosols: An overview, *J. Aerosol Sci.*, *27*(3), 359–382, 1996.

Shaw, G E., Sun photometry, *Bull Am Meteorol. Soc.*, *64*, 4–10, 1983.

Thome, K. J., B. M. Herman, and J. A. Reagan, Determination of precipitable water from solar transmission, *J Appl Meteorol.*, *31*, 157–165, 1992.

Twomey, S., Aerosols, clouds and radiation, *Atmos Environ.*, *25*(A), 2435–2442, 1991.

Vermote, E., D. Tanré, J. L. Deuzé, M. Herman, and J. J. Morcrette, *Second Simulation of the Satellite Signal in the Solar Spectrum* (6S), user guide, Version 1, January 16, 1996.

Ward, D. E., R. A. Susott, J. B. Kauffman, R. E. Babbit, D. L. Cummings, B. Dias, B. N. Holben, Y. J. Kaufman, R. A. Rasmussen, and A. W. Setzer, Smoke and fire characteristics for cerrado and deforestation burns in Brazil: BASE B experiment, *J. Geophys. Res.*, *97*, 14,601–14,619, 1992.

R. N. Halthore, Brookhaven National Laboratories, DAS/ECD, Upton, NY 11973-5000. (e-mail: halthore@aerosol.das.bnl.gov)

B. N. Holben and B. L. Markham, NASA Goddard Space Flight Center, Code 923, Greenbelt, MD 20771. (e-mail: brent@kratmos.gsfc.nasa.gov; Brian_Markham@gsfc.nasa.gov)

J. S. Schafer, Hughes STX Corporation, Code 923, NASA-GSFC, Greenbelt, MD 20771. (e-mail: schafer@ltpmail.gsfc.nasa.gov)